nature photonics

LETTERS

PUBLISHED ONLINE: 14 DECEMBER 2008 | DOI: 10.1038/NPHOTON.2008.250

High *k*-space lasing in a dual-wavelength quantum cascade laser

Kale J. Franz[1]*, Stefan Menzel[1,2†], Anthony J. Hoffman[1], Dan Wasserman[1†], John W. Cockburn[2] and Claire Gmachl[1]

The understanding of charge carrier distributions is fundamental to our knowledge of laser systems. In semiconductor lasers, because of the propensity of charge carriers to undergo extremely fast momentum relaxation[1,2], they accumulate at band extrema—that is, they have a small wavevector close to $k \approx 0$ in direct-gap semiconductors. Conventional understanding suggests that the device-level physics occurs at these band extrema, including population inversion for lasing. This behaviour is universal in diode lasers[3,4], interband cascade lasers[5] and quantum cascade lasers[6,7]. Here, we report on a quantum cascade laser with an energy configuration able to establish local population inversion high in *k*-space. We observe dual-wavelength emission from two discrete optical transitions. Temperature-dependent performance attributes show that the two transitions are highly coupled; competition for charge carriers is apparent from the anti correlated behaviour. The two optical transitions represent a conventional quantum cascade laser transition at $k \approx 0$ and another laser transition from non-thermal electrons near $k \approx 3.6 \times 10^8$ m^{-1}.

Inventing new semiconductor lasers has fundamentally relied on methods for obtaining population inversion. For example, the first quantum cascade (QC) lasers[6] sought to maximize inversion despite compromising oscillator strength; they used spatially delocalized energy states populated with quasi-equilibrium electrons. Other less traditional methods have also been used to realize semiconductor injection lasers. Laser transitions with one state comprising a virtual state have been demonstrated using both Bloch gain[8,9] and stimulated Raman scattering[10]. Even in such cases, however, inversion is achieved using electron populations in quasi-equilibrium, thermally distributed around the Γ point.

Hot-hole (p-Ge) lasers[11,12] are an exception in that they diverge from the standard semiconductor laser configuration. Here, a combination of large crossed electric and magnetic fields preferentially populates the light hole band by trapping carriers in cyclotron orbits at high *k*-space, while the applied electric field sweeps holes out of the heavy hole band through streaming motion[13]. Once these streaming holes in the heavy hole band reach the energy of an optical phonon, a scattering path opens where they can then repopulate the light hole band.

In the work presented here, instead of using externally applied electric and magnetic fields, we use intrinsic scattering processes (that is, the momentum transfer associated with optical phonons) to populate an energy sub-band high in *k*-space. Thermally distributed quasi-equilibrium electrons are injected into a lower energy sub-band at high *k*-space values. Population inversion for these 'hot' electrons is achieved through the properties of intra- and intersub-band scattering.

The high *k*-space lasing reported here was discovered in a QC laser that uses highly excited states for the optical transition[14]. (Two notable examples of other QC excited-state lasers are found in refs 15 and 16.) In our two-well active-region design, for which the conduction band energy diagram is shown in Fig. 1a, the primary optical transition is between the energy states labelled $|5\rangle$ and $|4\rangle$; a conventional two-well QC laser design would use the states $|3\rangle$ and $|2\rangle$ for the optical transition. A result of electrically injecting into highly excited active region states is that additional lower-lying energy levels and transitions with large oscillator strengths exist . Below the states of the $|5\rangle \rightarrow |4\rangle$ optical transition are three active-region energy levels. With electron injection high in the active-region structure, these other levels are candidates for supporting additional optical transitions.

We observe two distinct optical transitions in the spontaneous emission spectrum: one at $\lambda \approx 9.5$ μm (near the original $|5\rangle \rightarrow |4\rangle$ design wavelength of 9.7 μm) and one at 8.2 μm, as shown in Fig. 1b for devices at 80 K. With ridge laser structures at 80 K, we find that these transitions lase simultaneously; similar threshold currents are observed at this temperature. We have previously identified[14] the 9.5 μm emission as originating from transition $|5\rangle \rightarrow |4\rangle$ and the 8.2 μm emission originating from transition $|4\rangle \rightarrow |2\rangle$, based on the resonant wavelengths of the emission spectrum and the unique field-dependent behaviour of the optical emission.

A complete investigation of the temperature and current dependence of the emission reveals that each of the two transitions has distinctive temperature-dependent characteristics. Light from the $|5\rangle \rightarrow |4\rangle$ transition shows a behaviour typical of a QC laser intersub-band optical transition. As indicated in Fig. 2a,c, the highest output power and lowest threshold currents are achieved at low temperatures. With increasing temperature, shorter non-radiative transition times, thermal population of the lower laser state, thermionic emission from the upper laser state, and decreased upper laser level injection efficiency make obtaining population inversion more difficult. Consequently, stronger pumping is required to achieve laser action, until a temperature is reached where the laser is unable to achieve threshold, in this case near 125 K. (Although QC lasers routinely surpass room-temperature operation, high thermal performance is not expected in this case due to the proximity of state $|5\rangle$ to the barrier band edge and the associated thermally induced current leakage.)

The lower $|4\rangle \rightarrow |2\rangle$ transition, however, deviates from the familiar intersub-band optical transition behaviour significantly. Most strikingly, the transition lases more effectively at elevated temperatures (near 100 K), whereas performance is significantly diminished at lower temperatures. As shown in Fig. 2b,c for a 1.48 mm × 12.1 μm device, lasing onset is induced near 60 K. Peak output power with

[1]Department of Electrical Engineering, Princeton University, Princeton, New Jersey 08544, USA, [2]Department of Physics and Astronomy, University of Sheffield, Sheffield S3 7RH, UK; †Present address: Institute for Photonic Microsystems, Fraunhofer Society, D-01109 Dresden, Germany (S.M.); Department of Physics, University of Massachusetts, Lowell, Massachusetts 01854, USA (D.W.); *e-mail: kfranz@princeton.edu

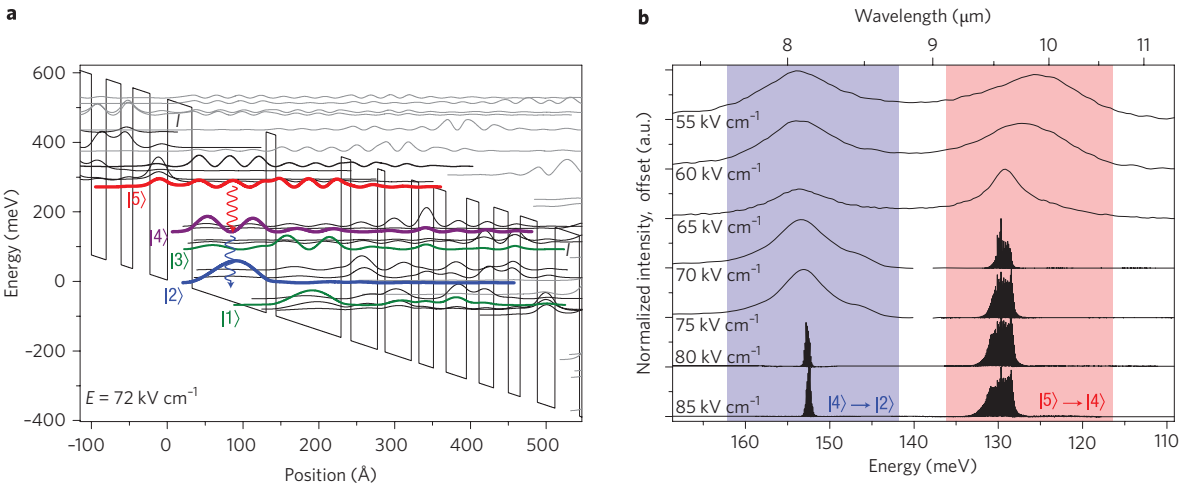

Figure 1 | Excited-state QC laser band diagram and emission spectra. a, A portion of the conduction band energy diagram for our QC structure, composed of interleaved $Al_{0.48}In_{0.52}As$ barriers and $In_{0.53}Ga_{0.47}As$ quantum-well layers. The conduction band edge is shown at an applied electric field $E = 72$ kV cm^{-1}. The quantized sub-band energies and the associated wavefunctions (squared moduli) are also shown. Five key active-region sub-bands are labelled, with optical transitions identified as $|5\rangle \rightarrow |4\rangle$ and $|4\rangle \rightarrow |2\rangle$, and indicated by red and blue wavy arrows, respectively. The $|4\rangle \rightarrow |2\rangle$ optical transition occurs high in *k*-space, as is shown later in Fig. 3b. **b**, Emission spectra for one QC laser at 80 K. Electroluminescence is followed by laser action as the applied electric field and pumping current are increased. We identify transition $|5\rangle \rightarrow |4\rangle$ as the source of the $\lambda \approx 9.5$ μm emission and transition $|4\rangle \rightarrow |2\rangle$ as the source of the 8.2 μm emission.

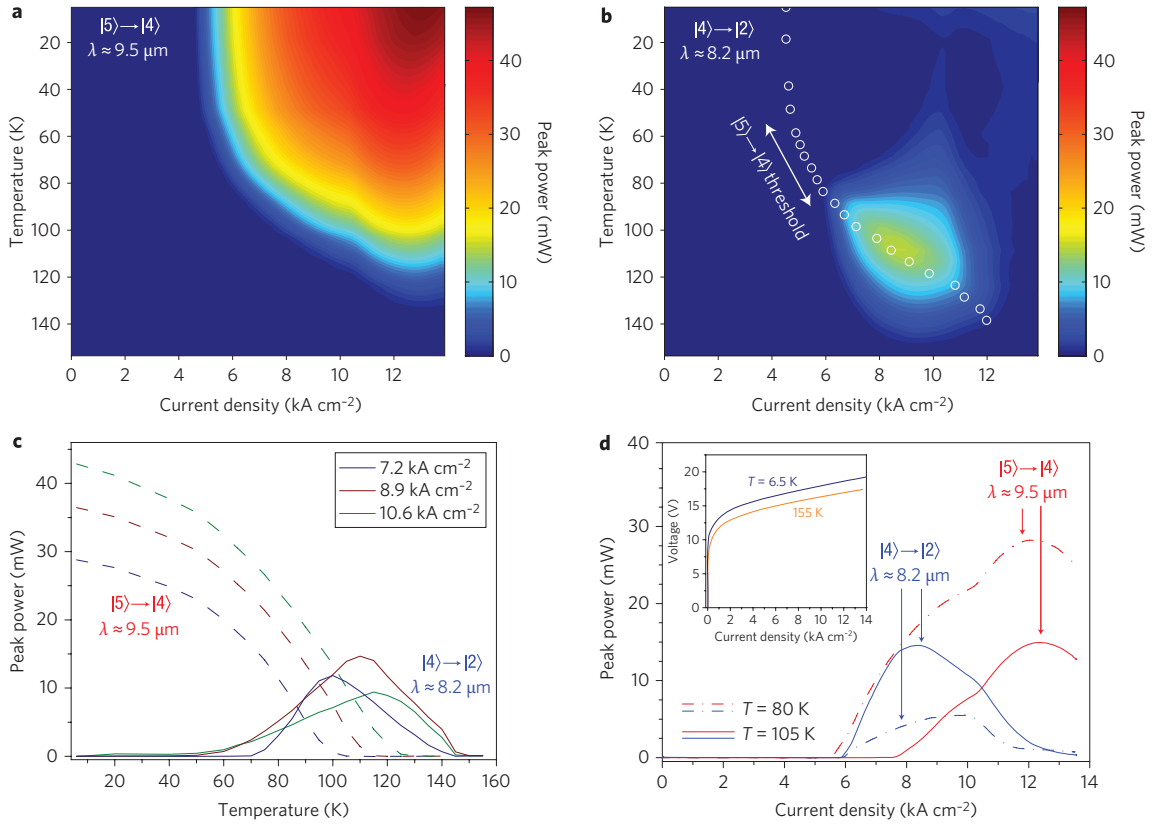

Figure 2 | Light output characteristics of a representative device. a,**b**, Light output versus current density and heat sink temperature of a 1.48 mm × 12.1 μm laser for the light at wavelengths of ~9.5 μm (**a**) and ~8.2 μm (**b**). Data shown for the $|5\rangle \rightarrow |4\rangle$ transition are consistent with standard QC laser behaviour. In contrast, the $|4\rangle \rightarrow |2\rangle$ transition operates poorly at the lowest heat sink temperatures; the transition instead has a thermally induced peak performance near 115 K. With the $|5\rangle \rightarrow |4\rangle$ transition threshold (white circles) overlaid on **b**, it can be seen that the $|4\rangle \rightarrow |2\rangle$ transition power roll-off is coincident with $|5\rangle \rightarrow |4\rangle$ turn-on. **c**, Spectrally resolved light output for three fixed pumping current densities with increasing temperature. The $|5\rangle \rightarrow |4\rangle$ transition is shown with dashed lines and the $|4\rangle \rightarrow |2\rangle$ transition is shown with solid lines. The $|4\rangle \rightarrow |2\rangle$ transition output is affected by the $|5\rangle \rightarrow |4\rangle$ transition output power. **d**, Light–current curves for each optical transition at 80 and 105 K. A crossover in laser thresholds occurs at 85 K, where the $|4\rangle \rightarrow |2\rangle$ transition achieves a lower threshold than the $|5\rangle \rightarrow |4\rangle$ transition. At 105 K, transition $|4\rangle \rightarrow |2\rangle$ has the lower threshold; here, the $|5\rangle \rightarrow |4\rangle$ transition threshold marks the beginning of the $|4\rangle \rightarrow |2\rangle$ power roll-off. Inset: current–voltage curves for 6.5 and 155 K heat sink temperatures.

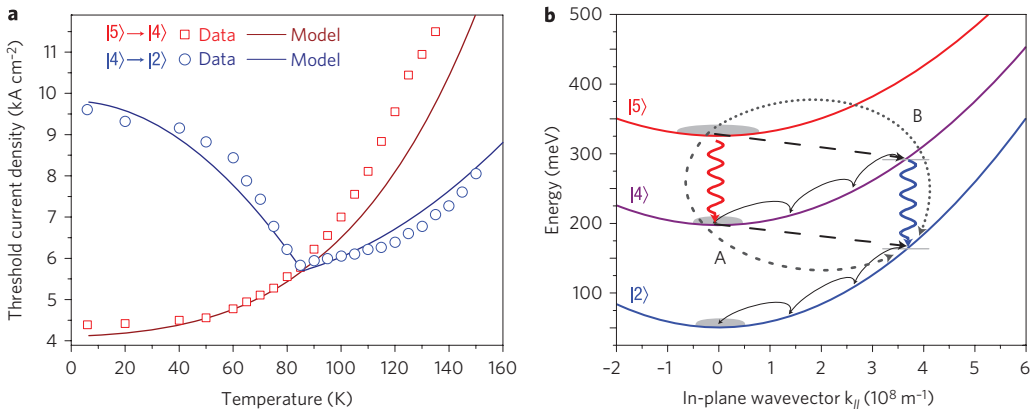

Figure 3 | Model results and *k*-space representation. a, Observed and modelled temperature-dependent threshold current densities for the two optical transitions. Red symbols indicate thresholds for the $|5\rangle \rightarrow |4\rangle$ transition and blue symbols the $|4\rangle \rightarrow |2\rangle$ transition. A crossover in thresholds is seen near 85 K. Before this crossover, the $|4\rangle \rightarrow |2\rangle$ transition threshold decreases with increasing temperature. A sharp kink is observed in the $|4\rangle \rightarrow |2\rangle$ threshold when it becomes lower than that of transition $|5\rangle \rightarrow |4\rangle$. These features are reproducible with a conventional QC rate-equation model with temperature-dependent parameters[19], the results of which are indicated by solid lines. **b**, A schematic representation of the high *k*-space lasing. The *k*-space dispersion of the sub-bands $|5\rangle$, $|4\rangle$ and $|2\rangle$ is shown. Electrons being injected into state $|5\rangle$ can follow either path A (the $|5\rangle \rightarrow |4\rangle$ optical transition) or path B (the $|4\rangle \rightarrow |2\rangle$ optical transition preceded by LO phonon scattering). Path A is typical for a QC laser transition, and path B represents the high *k*-space transition. Optical transitions are indicated by wavy arrows, intersub-band phonon transitions are shown with dashed-line arrows, intrasub-band scattering is shown with curved arrows, and paths A and B are shown with dotted arrows.

constant current density, contrary to expectation, increases with temperature up to 115 K, while threshold current simultaneously decreases. For temperatures above 115 K, a more typical thermal roll-over in power is observed. The light–current curves in Fig. 2d reveal more: a threshold 'crossover' is observed at 85 K, above which point the $|4\rangle \rightarrow |2\rangle$ transition develops a lower threshold than the $|5\rangle \rightarrow |4\rangle$ transition. At temperatures below this crossover, if the $|4\rangle \rightarrow |2\rangle$ transition is lasing, the $|5\rangle \rightarrow |4\rangle$ transition is also lasing. After the crossover and for low pumping rates, a regime exists where only the lower $|4\rangle \rightarrow |2\rangle$ transition lases. However, as soon as the upper $|5\rangle \rightarrow |4\rangle$ transition reaches threshold, an abrupt drop in $|4\rangle \rightarrow |2\rangle$ output power is observed. This anticorrelation in output power between the two transitions persists even above threshold. In Fig. 3a a plot of thresholds shows that, after crossover, the $|4\rangle \rightarrow |2\rangle$ transition threshold takes on a typical QC laser behaviour, having a characteristic temperature $T_0 \approx 220$ K. Before crossover, however, the transition has a negative characteristic temperature $T_0 \approx -64$ K. The sharp kink in the $|4\rangle \rightarrow |2\rangle$ transition threshold at the crossover point along with the anticorrelated output power behaviour are indicative of the strong interaction between the carrier populations of the two optical transitions.

We used standard laser rate equations with stimulated emission terms to model a system with two optical transitions, including temperature-dependent parameters where appropriate. The models show that population inversion for the $|4\rangle \rightarrow |2\rangle$ transition is not feasible with a practical parameter set for a purely stacked transition scheme where both transitions lase from the Γ point ($k = 0$). Sequential transitions would also prohibit the observed anticorrelated behaviour; here, stronger $|5\rangle \rightarrow |4\rangle$ population inversion would lead to stronger $|4\rangle \rightarrow |2\rangle$ population inversion, contrary to what is observed. The data instead directly lead to a scheme in which a second optical transition is in competition with a first transition for charge carriers. In a QC structure such as ours, we arrive at the model schematically depicted in Fig. 3b, in which the second laser transition is a vertical transition between sub-bands, positioned high in *k*-space. Given the three identified energy sub-bands $|5\rangle$, $|4\rangle$ and $|2\rangle$, several different electron transport paths are possible; two are labelled A and B. Path A is characteristic for a QC laser optical transition, where electrons undergo a radiative transition followed by longitudinal optical (LO) phonon scattering. When the $|5\rangle \rightarrow |4\rangle$ transition is lasing, large cavity photon densities at 9.5 μm and strong stimulated emission ensure that this is the dominant electron path. However, at elevated temperatures, path B becomes available with increased LO phonon scattering out of state $|5\rangle$, populating state $|4\rangle$ high in *k*-space[17], in this case near $k = 3.6 \times 10^8$ m^{-1}. In the situation where path A is 'off' because threshold has not yet been reached for the $|5\rangle \rightarrow |4\rangle$ transition, lasing can then occur at high *k*-space for the $|4\rangle \rightarrow |2\rangle$ transition. If at any time path A turns on, path B and therefore $|4\rangle \rightarrow |2\rangle$ population inversion is suppressed because (a) fewer electrons are available to populate the upper state of the high *k*-space $|4\rangle \rightarrow |2\rangle$ optical transition and (b) electrons are injected into the lower state of the high *k*-space $|4\rangle \rightarrow |2\rangle$ transition. Moreover, if transport through path A is slowed due to a weakening $|5\rangle \rightarrow |4\rangle$ laser transition, path B will concurrently see an enhancement of available electrons able to contribute to $|4\rangle \rightarrow |2\rangle$ lasing. This effect accounts for the dramatic decrease in $|4\rangle \rightarrow |2\rangle$ threshold from 60 to 80 K. The observed anticorrelated behaviour of the two transitions is thus sustained. In this way, only local[18] *k*-space population inversion is achieved for the $|4\rangle \rightarrow |2\rangle$ transition, and global population inversion is not required.

Our rate-equation model thus includes seven energy levels: five for each of the active-region energy levels labelled in Fig. 1a and two high in *k*-space for sub-bands $|4\rangle$ and $|2\rangle$. The temperature dependence of energy state lifetimes[7], gain[19], injection efficiency, thermal backfilling of energy states[7] and thermionic emission[20] were all included. Figure 3a illustrates how the model is able to accurately reproduce three key features of the observed data: (a) the unconventional threshold behaviour of the $|4\rangle \rightarrow |2\rangle$ laser transition that decreases then increases with temperature; (b) the crossing of the $|5\rangle \rightarrow |4\rangle$ and $|4\rangle \rightarrow |2\rangle$ laser thresholds; and (c) the sharp kink in the temperature-dependent evolution of the $|4\rangle \rightarrow |2\rangle$ transition threshold at the crossover point.

Of particular interest for such a high *k*-space transition is the effect of energy sub-band non-parabolicity[17]. At the Brillouin zone centre $k = 0$, energy sub-bands have a substantially parabolic form. However, with both increasing *k* and increasing sub-band energy above the band edge, the sub-bands flatten[21]. This non-parabolicity has spectral consequences: for the $|4\rangle \rightarrow |2\rangle$ transition in our structure, we calculate that photons generated at

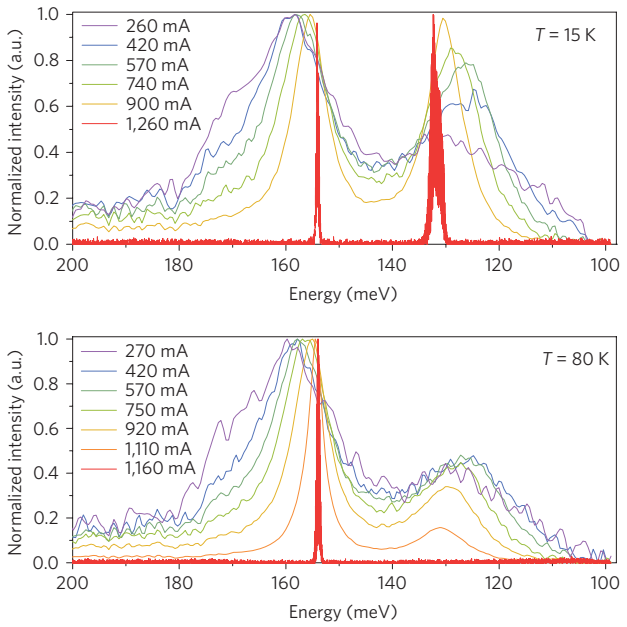

Figure 4 | Spectral signature of *k*-space emission. Spectral behaviour of a 1.93 mm × 9.4 μm laser at 15 and 80 K, with $|4\rangle \rightarrow |2\rangle$ transition emission centred around 160 meV. Resulting from sub-band non-parabolicity, high *k*-space emission has less photon energy than emission from $k = 0$. For the $|4\rangle \rightarrow |2\rangle$ transition, the broad emission with pronounced asymmetry at low injection currents is indicative of optical emission originating from a distribution of *k* values. As the injection current increases, the transition preferentially emits photons at the low-energy edge of the distribution—that is, from high in *k*-space.

$k = 3.6 \times 10^8$ m^{-1} will have 16.1 meV less energy than photons generated at $k = 0$. Subthreshold spectral data, as shown in Fig. 4 for a 1.93 mm × 9.4 μm laser, reveal such a *k*-space spectral signature. For the $|4\rangle \rightarrow |2\rangle$ emission around 160 meV, we observe two effects that contribute to a spectral redshift. Over a range of injection currents that spans deeply subthreshold to just above threshold, Stark tuning shifts the peak emission by ~5.5 meV, as is common for vertical transition QC structures. More interestingly, at low injection currents, the $|4\rangle \rightarrow |2\rangle$ emission exhibits pronounced asymmetry. At the lowest injection currents, the spectral width is quite broad—about 15 meV. As injection current is increased, the higher energy side of the emission collapses, and the transition strongly favours emission on the side of low energy (that is, emission from higher up in the band). Also, as injection current is increased, the emission asymmetry gives way to a more typical Lorentzian-shaped emission. Thus, for a laser device where cavity effects strongly influence emission behaviour, these spectral features are consistent with laser emission originating high in *k*-space.

Non-parabolic energy sub-bands lead to two interesting and favourable consequences for a high *k*-space laser transition. First, threshold currents are reduced due to a decrease in the primary source of optical absorption loss—that is, intersub-band absorption at the lasing energy from the electron pool at $k = 0$. With a high *k*-space transition between non-parabolic energy sub-bands, the optical emission process is decoupled from the normally concurrent reverse process of optical absorption. Second, the presence of non-parabolicity helps achieve a more favourable lifetime profile for the $|4\rangle \rightarrow |2\rangle$ transition. Because of non-parabolicity, the energy conversion of an LO phonon requires the exchange of a larger wavevector *k* for higher energy sub-bands, which in turn reduces the scattering rate[2,22,23] as $1/k^2$ (refs 24,25). The influences of these effects are reflected in the results of our rate-equation model. To achieve a threshold-crossing-point at the temperature consistent with the data shown in Fig. 3a, the optical absorption loss associated with the $|4\rangle \rightarrow |2\rangle$ laser energy was decreased by about a factor of 10.

In conclusion, we have demonstrated a dual-wavelength QC structure that lases with one conventional ($\lambda \approx 9.5$ μm) and one high *k*-space ($\lambda \approx 8.2$ μm) optical transition. The QC laser shows dual-wavelength emission, with the high *k*-space transition being anticorrelated with the primary laser transition. A rate-equation model based on incorporating a high *k*-space optical transition reproduces characteristic features of the observed temperature-dependent emission behaviour. The demonstration of *k*-space lasing represents a departure from the conventional approaches to semiconductor lasers, presenting the possibility of designing intersub-band devices making more cognizant use of full *k*-space population distributions.

Methods

Laser growth and fabrication. The laser was grown using gas-source molecular beam epitaxy on an InP substrate. The active core contained 40 periods of the layer sequence (in ångströms starting from the injection barrier) **32**/98/**13**/86/**13**/35/**10**/35/**10**/20/**16**/27/**16**/20/**19**/16/**23**/23, where $In_{0.52}Al_{0.48}As$ barrier layers are in bold, $In_{0.53}Ga_{0.47}As$ well layers are in normal font and Si-doped (2×10^{17} cm^{-3}) layers are underlined. The active core was embedded in a conventional dielectric, InP-based waveguide. Full details of the device fabrication can be found in ref. 14.

Measurements and characterization. Spectra shown in Fig. 1b were collected using a Fourier-transform infrared (FTIR) spectrometer with 100-ns current pulses at 50 kHz. Electroluminescence spectra shown in Fig. 4 were taken using an FTIR in step scan mode with 8 cm^{-1} resolution. The temperature-dependent light–current measurements of Fig. 2 were taken with 100 ns current pulses at 5 kHz using a gated integrator and boxcar averager. A long-pass filter with cut-off at $\lambda = 8.65$ μm and a short-pass filter with cut-off at $\lambda = 8.70$ μm were used to spectrally resolve emission from the two transitions. For a thorough study of the structure, along with preliminary characterization of multiple (~30) laser devices, we performed full, detailed, temperature-dependent characterizations on six different lasers from different parts of the wafer. Cavity lengths were 1.38, 1.48, 1.50, 1.63, 1.93 and 2.28 mm. All devices showed similar anticorrelated behaviour between two competing optical transitions lasing near $\lambda \approx 9.5$ and 8.2 μm. In all cases, a stronger $|5\rangle \rightarrow |4\rangle$ transition always led to a weaker $|4\rangle \rightarrow |2\rangle$ transition.

Received 12 June 2008; accepted 14 November 2008; published online 14 December 2008

References

1. Rudin, S. & Reinecke, T. L. Electron LO-phonon scattering rates in semiconductor quantum wells. *Phys. Rev. B* **41,** 7713–7717 (1990).
2. Alcalde, A. M. & Weber, G. Nonparabolicity effects on electron-optical-phonon scattering rates in quantum wells. *Phys. Rev. B* **56,** 9619–9624 (1997).
3. Kroemer, H. Nobel Lecture: Quasielectric fields and band offsets: teaching electrons new tricks. *Rev. Mod. Phys.* **73,** 783–793 (2001).
4. Alferov, Z. I. Nobel Lecture: The double heterostructure concept and its applications in physics, electronics and technology. *Rev. Mod. Phys.* **73,** 767–782 (2001).
5. Olafsen, L. J., Vurgaftman, I. & Meyer, J. R. *Long-Wavelength Infared Semiconductor Lasers* (ed. Choi, H. K.) Ch. 3, 69–143 (Wiley, 2004).
6. Faist, J. *et al.* Quantum cascade laser. *Science* **264,** 553–556 (1994).
7. Gmachl, C., Capasso, F., Sivco, D. L. & Cho, A. Y. Recent progress in quantum cascade lasers and applications. *Rep. Prog. Phys.* **64,** 1533–1601 (2001).
8. Terazzi, R. *et al.* Bloch gain in quantum cascade lasers. *Nature Phys.* **3,** 329–333 (2007).
9. Revin, D. G. *et al.* Dispersive gain and loss in midinfrared quantum cascade laser. *Appl. Phys. Lett.* **92,** 081110 (2008).
10. Troccoli, M. *et al.* Raman injection laser. *Nature* **433,** 845–848 (2005).
11. Shastin, V. N. Hot hole inter-sub-band transition p-Ge FIR laser. *Opt. Quantum Electron.* **23,** S111–S131 (1991).
12. Bründermann, E. *Long-Wavelength Infared Semiconductor Lasers* (ed. Choi, H. K.) Ch. 6, 279–350 (Wiley, 2004).
13. Pinson, W. E. & Bray, R. Experimental determination of the energy distribution functions and analysis of the energy-loss mechanisms of hot carriers in p-type germanium. *Phys. Rev.* **136,** A1449–A1466 (1964).
14. Franz, K. J. *et al.* Evidence of cascaded emission in a dual-wavelength quantum cascade laser. *Appl. Phys. Lett.* **90,** 091104 (2007).
15. Sirtori, C. *et al.* Dual-wavelength emission from optically cascaded intersubband transitions. *Opt. Lett.* **23,** 463–465 (1998).
16. Scalari, G. *et al.* Electrically switchable, two-color quantum cascade laser emitting at 1.39 and 2.3 THz. *Appl. Phys. Lett.* **88,** 141102 (2006).

17. Serapiglia, G. B., Vodopyanov, K. L. & Phillips, C. C. Nonequilibrium electron distributions in a three-subband InGaAs/InAlAs quantum well studied via double resonance spectroscopy. *Appl. Phys. Lett.* **77,** 857–859 (2000).
18. Faist, J. *et al.* Quantum cascade lasers without intersubband population inversion. *Phys. Rev. Lett.* **76,** 411–414 (1996).
19. Faist, J. *et al. Semiconductors and Semimetals* (eds Liu, H. C. & Capasso, F.) Vol. 66, p. 36 (Academic Press, 2000).
20. Sze, S. *Physics of Semiconductor Devices* (John Wiley & Sons, 1981).
21. Sirtori, C., Capasso, F., Faist, J. & Scandolo, S. Nonparabolicity and a sum-rule associated with bound-to-bound and bound-to-continuum intersubband transitions in quantum-wells. *Phys. Rev. B* **50,** 8663–8674 (1994).
22. Ridley, B. K. *Quantum Processes in Semiconductors* 4th edn (Oxford Univ. Press, 1999).
23. Sinning, S. *et al.* Reduced subpicosecond electron relaxation in GaN_xAs_{1-x}. *Appl. Phys. Lett.* **86,** 161912 (2005).
24. Harrison, P. *Quantum Wells, Wires and Dots: Theoretical and Computational Physics of Semiconductor Nanostructures* 2nd edn (Wiley, 2005).
25. Bockelmann, U. & Bastard, G. Phonon scattering and energy relaxation in two-, one- and zero-dimensional electron gases. *Phys. Rev. B* **42,** 8947–8951 (1990).

Acknowledgements

The authors gratefully acknowledge helpful comments, advice and support from J. Chen, F.-S. Choa, S. R. Forrest, S. Gooding, K.-T. Shiu, I. Waldmueller and Y. Yao. This work was supported in part by the Mid-Infrared Technologies for Health and the Environment (MIRTHE) centre (NSF-ERC no. EEC-0540832) and the European Union Marie Curie Research Training Network Physics of Intersubband Semiconductor Emitters (POISE) programme. K.J.F. gratefully acknowledges the support of the National Science Foundation Graduate Research Fellowship Program.

Additional information

Reprints and permission information is available online at http://npg.nature.com/reprintsandpermissions/. Correspondence and requests for materials should be addressed to K.J.F.